Petroleum and Coal

Article **Open Access**

Macroscopic Two-Dimensional Two-Fluid Eulerian- Eulerian Model for Tracking the Evolution of Solid and Gaseous Phases in a FCC Riser Reactor

Anatoliy Vorobev[1], Artem Antonov[2], Galina Nazarova[2], Elena Ivashkina[2], Emiliya Ivanchina[2], Vyacheslav Chuzlov[2], Toleubek Kaliev[2,3,4]*

[1] *University of Southampton, United Kingdom*
[2] *National Research Tomsk Polytechnic University, Russia*
[3] *National Research Tomsk Polytechnic University, Russia*
[4] *Toraighyrov Pavlodar State University, Republic of Kazakhstan*

Received August 31, 2021; Accepted December 22, 2021

Abstract

This study presents the development of a macroscopic three-dimensional two-fluid Eulerian- Eulerian model for tracking the evolution of solid and gaseous phases in a Fluid Catalytic Cracking (FCC) riser, with a zeolite catalyst and the petroleum feedstock being modelled respectively as the continuous solid and gaseous phases. The solid phase was modelled by using the kinetic theory of granular flow (KTGF) for particulate phases. By using the commercial software ANSYS Fluent, the Computational Fluid Dynamics (CFD) investigation of the gas-solid hydrodynamics within the catalytic cracking riser was carried out. The aim was to develop a computational hydrodynamic model and to illustrate the work of the new model by examining the several fluidized beds with gradually increasing complexity. Overall, the results obtained for the simplified designs show similarities to the operation of a real-life FCC unit. The achieved outcomes will be valuable for further improvements of modern FCC risers.

Keywords: *Catalytic cracking; Computational fluid dynamics; Kinetic theory of granular flow; Riser reactor.*

1. Introduction

Catalytic cracking (FCC) is the most commonly used process when the long chain vacuum gas oil hydrocarbons breakdown to lighter and more commercially useful products such as gasoline, diesel and light olefins (ethylene and propylene), which are used for the plastics production. To research and develop the processes and technologies of the oil and gas industry, a computational fluid dynamics are widely used. In recent years, the development of CFD software has enabled to perform three-dimensional simulations of fluidized bed of catalyst solids, including both hydrodynamics and reaction kinetics, in recent years. During the last twenty years, CFD tools have become more popular for modeling the hydrodynamic behavior of the fluidized beds [1]. Wickman and Nays [2] proposed the first three-component kinetic model. Hydrocarbons substances are divided to components called lumps: feedstock, gasoline and the other component (light gases and coke) which was remained. This model combines the coke and light gases as the same pseudo-component; therefore, the coke deposited on the catalyst and the mass transfer from the gas phase to the solid are ignored when the model are created. Jacob *et al.* [3] later created a ten-lump kinetic model which includes 'dry gas' component. Moreover, the authors attempted to describe undesirable thermal cracking reactions which occurred in the high temperature part of the riser. A list of papers is dedicated to kinetics and thermodynamics of the industrial FCC process [4-8].

Application of the advanced CFD software presents in the recent models, which produces more accurate results. This helps to achieve more cheaper and less time-consuming results to understand and analyzes. Eleven-lumps model was designed by Gan *et al.* [9] to give the companies to meet manufacturing demand when propylene market fast-grows. The model

allows them to maximize the yield of propylene. The more recent study which focuses on maximizing propylene production performed by Young *et al.* [10] demonstrates the use of the latest version of ANSYS Fluent software. This allowed them to import of user-defined functions written by C programming language to create an extremely accurate kinetic model which includes eleven-lumps.

A three-phase model which considers a three-dimensional flow of a gas, liquid and solid, heat transfer, evaporation of droplets and chemical reactions, was created [11]. The authors chose Eulerian approach, since the equations for the position of the temperature velocity and particle mass were solved for each discrete particle. During the study how, the feedstock injection influences the mixing, the authors [12] revealed that the intensive mixing accelerates the mass transfer and increases the yield of the desired products. Due to a short time, the prolonged contact between catalyst and feedstock are avoided, that keeps the desired products from further cracking and coking reactions. The perfect variant to organize the desired flow and reactions is 30°.

Moreover, the studies, which include a fully developed flow in FCC Risers, are not so many. Huang *et al.* [13] created the development of flow and measured particle velocity and solid particle retention by experimental study using fiber optic probes. To create a lump-free kinetic model and study flow evolution, Idris and Berne [14] used ANSYS CFX. However, the geometries was far from real FCC risers in these two studies when height and wide of the modeled column was 15.1 and 0.1 m which was approximately half and about 10% of the actual riser height and width. This made it easier to study the development of the flow, since the cross section is too narrow.

The aim of this study is to develop a macroscopic three-dimensional two-fluid Eulerian-Eulerian model for tracking the evolution of zeolite catalyst and the petroleum feedstock being modeled respectively as the continuous solid and gaseous phases in a FCC riser

2. Mathematical model

To study the hydrodynamics of the riser from S-200 KT-1/1 industrial unit, we carried out a three-dimensional modeling of a reactive two-phase flow using two-fluid Eulerian-Eulerian model. The gaseous oil and solid catalytic phases are considered as interpenetrating continua, since we chose Eulerian model. For both phases, volume fractions with the sum of one are introduced and we assume that they are continuous functions of time and space.

At this stage, we do not take into account the chemical reactions which occur in riser. The main aim of this study is to compare our simplified approach with an extensive hydrodynamic model, which includes the complicated 11-lump kinetic model previously developed by Young *et al.* [10] to maximize propylene production (one of a main challenge for FCC units due to current demand). Both models use a two-fluid Eulerian- Eulerian approach to simulate the hydrodynamics of riser, the catalyst is modeled as a granular phase, the properties of this phase are derived from KTGF.

The conservation equations of solid phase are closed using constitutive equations derived from the kinetic theory of granular flow (KTGF). Importantly, that the liquid phase is absents at the inlet of the riser, the feedstock is supplied to the model completely evaporated at the nozzles inlet. This is justified by the fact that the time required for complete evaporation in typical FCC units varies from 0.3 to 30.0 ms [15] when a droplet size is 100 μmm, which is much shorter than the residence time of the feedstock in typical industrial risers (3–4 s).

Using the form of governing equations, which is averaged in each computational cell to achieve mean fields, allows us to study the physics of dispersed flows and particle-particle interactions. The conservation equations, when Eulerian model is used, are solved separately for the solid and gas phases. The Navier-Stokes equation is used to represent how the gas and fluidized particles move [16].

2.1. Conservation equations

Mass-conservation equation

Conservation equations can be derived by ensemble averaging of the local instantaneous balance for each phase [17].

The balance equation for the volume fraction is:

$$\varepsilon_g + \varepsilon_s = 1 \quad (1)$$

here ε_g - the volume fraction of the gaseous phase; ε_s - the volume fraction of the solid phase.

The continuity equations of the gaseous and solid phases are determined respectively:

$$\frac{\partial}{\partial t}(\varepsilon_g \rho_g) + \nabla \cdot (\varepsilon_g \rho_g \vec{v}_g) = 0 \quad (2)$$

$$\frac{\partial}{\partial t}(\varepsilon_s \rho_s) + \nabla \cdot (\varepsilon_s \rho_s \vec{v}_s) = 0 \quad (3)$$

Impulse-conservation equations

Impulse-conservation equations for both phases were related by the interphase exchange parameters, which are determined accordingly:

$$\frac{\partial}{\partial t}(\varepsilon_g \rho_g \vec{v}_g) + \nabla \cdot (\varepsilon_g \rho_g \vec{v}_g \vec{v}_g) = -\varepsilon_g \nabla P + \varepsilon_g \rho_g \vec{g} + \nabla \cdot \tau_g - \beta_{gs}(\vec{v}_g - \vec{v}_s) \quad (4)$$

$$\frac{\partial}{\partial t}(\varepsilon_s \rho_s \vec{v}_s) + \nabla \cdot (\varepsilon_s \rho_s \vec{v}_s \vec{v}_s) = -\varepsilon_s \nabla P + \varepsilon_s \rho_s \vec{g} + \nabla \cdot \tau_s - \beta_{gs}(\vec{v}_s - \vec{v}_g) \quad (5)$$

here β – impulse interphase transfer modelled by the Gidaspow drag model.

This combines the Wen Yu correlation with the Ergun equation. For dense areas of the solid phase (where ε_s> 0,26), β is calculated using:

$$\beta = 150 * \frac{\varepsilon_s^2 \mu_g}{\varepsilon_g d_s^2} + \frac{7}{4} \frac{|\vec{v}_s - \vec{v}_g| \varepsilon_s \rho_g}{d_s} \quad (6)$$

For diluted areas (where ε_s< 0,26) is defined using:

$$\beta = \frac{3}{4} C_d \frac{|\vec{v}_s - \vec{v}_g| \varepsilon_s \varepsilon_g \rho_g}{d_s} \omega, \quad (7)$$

$$\omega = \begin{cases} -0{,}576 + \dfrac{0{,}0214}{4(\varepsilon_g - 0{,}7463)^2 + 0{,}0044} & (0{,}74 \le \varepsilon_g \le 0{,}82) \\ -0{,}0101 + \dfrac{0{,}0038}{4(\varepsilon_g - 0{,}7789)^2 + 0{,}004} & (0{,}82 \le \varepsilon_g \le 0{,}97) \\ -31{,}8295 + 32{,}8295\varepsilon_g & (\varepsilon_g > 0{,}98) \end{cases} \quad (8)$$

here d_s – particle diameter (we assumed that all particles have the same diameter).

For solid particles when Reynolds number is large enough (Re> 1000) to dominate inertial over viscous effects, the drag coefficient C_d does not depended on Reynolds number In this case, this coefficient is calculated using the formula:

$$C_d = \frac{0{,}44}{\varepsilon_s^{1{,}65}} \quad (9)$$

If Reynolds number is less than 1000 (Re <1000), both inertial and viscous effects must be considered. The drag coefficient is depended on the Reynolds number and determined by the following equation:

$$C_d = \frac{1}{\varepsilon_s^{1{,}65}} \frac{24}{Re}(1 + 0{,}15 Re^{0{,}687}) \quad (10)$$

Energy-conservation equation

To describe the energy conservation in Eulerian multiphase models, a separate enthalpy equation is written for each phase:

$$\frac{\partial}{\partial t}(\alpha_g \rho_g) + \nabla \cdot (\alpha_g \rho_g \vec{u}_g h_g) = \alpha_g \frac{\partial p_g}{\partial t} + \bar{\bar{\tau}}_g : \nabla \vec{u}_g - \nabla \vec{q}_g + \sum_{p=1}^{n} (Q_{sg} + \dot{m}_{sg} h_{sg} - \dot{m}_{gs} h_{gs}) \quad (11)$$

$$\frac{\partial}{\partial t}(\alpha_s\rho_s h_s) + \nabla\cdot(\alpha_s\rho_s\vec{u}_s h_s) = \alpha_s\frac{\partial p_s}{\partial t} + \bar{\bar{\tau}}_s:\nabla\vec{u}_s - \nabla\vec{q}_s + \sum_{p=1}^{n}(Q_{gs} + \dot{m_{gs}}h_{gs} - \dot{m_{sg}}\,h_{sg}) \quad (12)$$

here $h_{g,s}$ – specific enthalpy of the phases; $\vec{q}_{g,s}$ – heat flow of the phases; Q_{sg}, Q_{gs} - the heat exchange capacity between phases; h_{sg} – interphase enthalpy.

Heat transfer between phases must comply with the local balance conditions: $Q_{sg} = -Q_{gs}$ и $Q_{gg} = 0$

Constitutive equation

To close the conservation of momentum, establishment of the laws of the stress tensor for both phases is required. The properties of the dispersed phase were obtained on the basis of KTGF [16]. These properties include the pressure and viscosity of the granular phase. Solving the transfer equation gives the equation of granules temperature conservation (the fluctuation energy of the granular phase),θ_s

$$\frac{3}{2}\left[\frac{\partial}{\partial t}(\rho_s\varepsilon_s\theta_s) + \nabla(\rho_s\vec{v}_s\varepsilon_s\theta_s)\right] = (-P_s I + \tau_s)\nabla\vec{v}_s - \nabla\left(k_{\theta_s}\nabla\theta_s\right) - \gamma_s\theta_s + \phi_{gs} \quad (13)$$

here k_{θ_s}- thermal diffusion coefficient; $\gamma_s\theta_s$ - collision dissipation energy; ϕ_{gs} - kinetic energy transfer between gas and dispersed phases; $k_{\theta_s}$is defined as following:

$$k_{\theta_s} = \frac{2k_{dil}}{(1+e)g_0}\left[1 + \frac{6}{5}g_0\varepsilon_s(1+e)\right]^2 + 2\varepsilon_s^2\rho_s d_s(1+e)g_0\left(\frac{\theta}{\pi}\right)^{\frac{1}{2}} \quad (14)$$

here

$$k_{dil} = \frac{75\sqrt{\pi}}{384}\rho_s d_s\theta_s^{\frac{1}{2}} \quad (15)$$

$$g_0 = \frac{1}{1-\left(\frac{\varepsilon_s}{\varepsilon_s,max}\right)^{\frac{1}{3}}}, \varepsilon_s, max = 0{,}63 \quad (16)$$

here g_0 –, which is equal to the probability of collision between individual particle and another particle in the granular phase.

Therefore, when the volume fraction of the dispersed phase rises, its density as well as the probability of collision of two separate solid particles increases. As a result this lead to increase in the radial distribution function g_0.

In addition, the collision dissipation energy $\gamma_s\theta_s$ is determined by the equation:

$$\gamma_s\theta_s = \frac{12(1-e^2)g_0}{d_s\sqrt{\pi}}\rho_s\varepsilon_s^2\theta_s^{\frac{3}{2}} \quad (17)$$

The pressure of the granular phase ρ_s was determined based on the KTGF, according to Lun et al. equation [14]:

$$\rho_s = \varepsilon_s\rho_s\theta_s[1 + 2g_0\varepsilon_s(1+e)] \quad (18)$$

The laws for stress tensors for the gaseous and dispersed phases respectively are defined:

$$\tau_g = \varepsilon_s\mu_g\left\{\left[\nabla\vec{v}_g + \left(\Delta\vec{v}_g\right)^T\right] - \frac{2}{3}\left(\nabla\vec{v}_g I\right)\right\}, \quad (19)$$

here I – unit tensor.

In addition,

$$\tau_s = \left[-\varepsilon_g\rho_s + \varepsilon_g\lambda_s(\nabla\vec{v}_s)\right]I + \varepsilon_s\mu_s\{\left[\nabla\vec{v}_s + \left(\Delta\vec{v}_g\right)^T\right] - \frac{2}{3}(\nabla\vec{v}_g I)\} \quad (20)$$

The proposed expression for the shear viscosity μ_s, due to its collisions and motion, is determined by the optional friction term, which we neglect this, the collision and the kinetic terms:

$$\mu_s = \mu_{s,fric} + \mu_{s,col} + \mu_{s,kin,gran} \quad (21)$$

here if the flow is too dense, for example, is close to the maximum seal limit., the frictional viscosity $\mu_{s,fric}$, can be neglected. Therefore,

$$\mu_{s,fric} = 0 \quad (22)$$

Collisional viscosity, $\mu_{s,col}$, is defined as:

$$\mu_{s,col} = \frac{4}{5}\varepsilon_s^2 d_s \rho_s g_0 (1+e)\left(\frac{\theta_s}{\pi}\right)^{\frac{1}{2}} \quad (23)$$

Kinetic viscosity, $\mu_{s,kin,gran}$, is calculated according to:

$$\mu_{s,kin,gran} = \frac{10\rho_s d_s \sqrt{\theta_s \pi}}{96(1+e)g_0}\left[1 + \frac{4}{5}g_0 \varepsilon_s (1+e)\right]^2 \quad (24)$$

Bulk viscosity parameter, λ_s is defined as following:

$$\lambda_s = \frac{4}{3}\varepsilon_s d_s \rho_s g_0 (1+e)\left(\frac{\theta_s}{\pi}\right)^{\frac{1}{2}} \quad (25)$$

We also assumed that the particles always collide without sticking to each other, avoiding particle agglomeration.

2.2. Stages of hydrodynamic modeling

To modelling we used the academic version of ANSYS Fluent 20.2 software. This software package allows us to solve the numerical discretization of the mass and impulse conservation equations and form by the finite volume method. Initially, we also create 3D geometries using Autodesk Inventor Professional 2017 which were later combined by ANSYS Meshing. The Solver tool allow us to establish the boundary conditions, phase and interactions properties which are necessary to obtain accurate FCC data

Selecting the geometry and mesh

To model, we built 3D geometry of the riser according to dimensions from the FCC industrial unit. The constructed geometry includes four nozzles (holes) for feedstock supplying, symmetrically located on each side of the riser (Fig. 1). Given that the feedstock supplies in an evaporated form to model, there is no need to build nozzles with real dimensions. The riser geometry has been simplified in comparison with actual dimensions:

1. The length of the nozzles was reduced from 1.523 m to 0.3 m;
2. Water vapor to feedstock spray is absent;
3. The length of the regenerated catalyst pipe is reduced twice (6.3 m) to improve convergence.

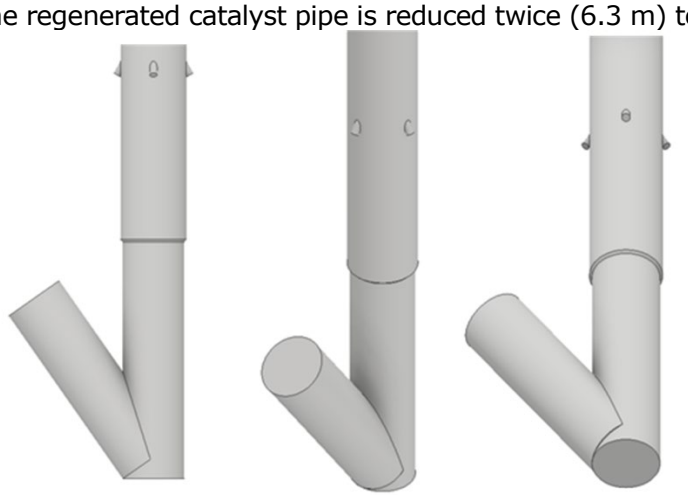

Figure 1. The lower part of the mixing unit of S-200, KT-1/1 catalytic cracking riser

Table 1 shows the geometric dimensions of the S-200, KT-1/1 catalytic cracking riser. Despite the entire riser was modeled in this study, we studed in detaled the feed injection zone and the lower conical expansion section with feed nozzles, since this part is characterized by

a complex interaction between the two phases. For mesh convergence purposes, two triangular meshes were initially tested, with a higher (248,741 cells and 50,656 nodes) and a lower density (122,584 cells and 25,422 nodes) (Table 2).

Table 1. Geometrical dimensions of S-200, KT-1/1 riser

Parameter	Value
Riser length, m	40.3
Riser diameter, m	1.3 (with rising up to 1.4)
Nozzle diameter, m	0.16
Nozzle length, m	0.3
Number of nozzles	4
Feedstock input angle, °	30
Diameter of the catalyst inlet pipe, m	1.3

Table 2. Comparison results of the tested meshes

Comparative parameter	Mesh #1	Mesh #2
A total number of cells	122 584	248 741
A total number of nodes	25 422	50 656
Maximum velocity of solid phase, m/s	72.36	73.29
Maximum velocity of gaseous phase, m/s	53.81	53.71

The calculations performed show insignificant discrepancies in the phase velocity and the volume fraction profiles. At the same time, the modelling using mesh #2 takes us twice time than mesh #1. Given that, we chose a mesh #1 for further calculations.

Phase properties

As mentioned earlier, a multiphase model with two Eulerian phases was created in this research. The gaseous phase was modeled as a mixture of liquids. Although its main component was gas oil vapor representing the feedstock, a total feedstock mixture also includes a second liquid represented by water vapor. Considering the vapor is necessary since this flow carries dispersed phase particles and accelerates them. Gasoil-vapor was chosen to simulate the feedstock since this material roughly reflects the average properties of the catalytic cracking feedstock from industrial unit. Detailed characteristics of gasoil-vapor and water-vapor are given in Tables 3, 4, respectively.

Table 3. Properties of the gasoil-vapor

Parameter	Value
Density (kg/m^3)	9.4
Viscosity (kg/ms)	7.00E-6
Cp (specific heat) (J/kgK)	2430
Thermal conductivity (W/mK)	0.0178
Molecular weight (kg/kmol)	221.16
Standard state enthalpy (J/kgmol)	3.30E+08
Reference temperature (K)	298.15

Table 4. Properties of the water-vapor

Parameter	Value
Density (kg/m^3)	0.5542
Cp (specific heat) (J/kgK)	Piecewise-polynomial
Thermal conductivity (W/mK)	0.0261
Viscosity (kg/ms)	1.34E-05
Molecular weight (kg/kmol)	18
Standard state enthalpy (J/kgmol)	-2.42E-08
Standard state entropy (J/kgmolK)	1.89E+05
Reference temperature (K)	298.15
L-J Characteristic length (angstroms)	2.605

The liquid dispersed phase has solid properties obtained using KTGF. The phase material consists of zeolite which is the main component of FCC catalysts. The density of this catalyst is 2100 kg/m^3. Particles of the granular phase were considered spherical, smooth, and inelastic. The detailed properties of zeolite are presented in Table 5.

Table 5. Zeolite material characteristics

Parameter	Value
Diameter (m)	8.00E-05
Granular viscosity (kg/ms)	1.00E-05
Granular bulk viscosity (kg/ms)	Lun-et-al
Frictional viscosity (kg/ms)	Johnson-et-al
Angle of internal friction (deg)	30
Frictional pressure (Pa)	Based-KTGF
Frictional modulus (Pa)	Derived
Friction packing limit (-)	0.61
Granular temperature (m^2/s^2)	Algebraic
Solids pressure (Pa)	Lun-et-al
Radial distribution (-)	Lun-et-al
Elasticity modulus (Pa)	Derived
Packing limit (-)	0.63

We selected the Gidaspow drag model and the Moraga lift model to define the drag and lift functions for each phase when considering phase interactions. In addition, the restitution coefficient for collisions between granular phases (zeolite – zeolite collisions) was chosen equal to 0.99, when the range of the restitution rate is 0.80–0.99 [16]. Selecting the highest value in this range simplifies the results. This led to a decrease in kinetic energy due to collisions. was chosen as an algebraic model of the interfacial region, we chose the ia – symmetric model, which considers the volume fractions of the primary (feedstock) and secondary (catalyst) phases to assess the interfacial region [17].

Operating and boundary conditions

A critical to getting realistic results determines the exact boundary conditions. Initially, to check the reliability of the hydrodynamic model calculation results, we used boundary conditions from Yang *et.al.* [10]. In addition, an outlet boundary hole was set to prevent overflow and the phase properties were kept constant throughout the modelling. To represent the flow on the walls of the lift-reactor, we applied the condition of the slip absence for gaseous phase, which was caused by existing a boundary layer near the wall. However, FCC fluid dynamics studies do not provide a clear understanding about the slip conditions which should be applied to the dispersed phase. In these simulations, a partial slip condition was chosen.

Options of modelling solver

The FCC riser was modelled using a pressure transient solver with an absolute velocity formulation. A simple scheme (SIMPLE) of the relationship between pressure and velocity was chosen as a method for solving the realized turbulent k-e model. The Under-relaxation factor was decreased to improve the convergence of the results. A full list of these solution methods and controls is shown in Tables 6-7.

Table 6. Parameters of the solution method used to development of the model

Pressure Velocity Coupling	Scheme	Pressure Coupled SIMPLE
Spatial Discretization	Gradient	Least Squares Cell Based
	Momentum	Second Order Upwind
	Volume Fraction	First Order Upwind
	Turbulent Kinetic Energy	First Order Upwind
	Turbulent Dissipation Rate	First Order Upwind
	Energy	First Order Upwind
	Transient Formulation	First Order Implicit

Table 7. The general parameters for solution used in modeling

Under-relaxation factors			
Pressure	0.3	Granular temperature	0.2
Density	1	Turbulent kinetic energy	0.8
Body forces	1	Turbulent dissipation rate	0.8
Momentum	0.05	Turbulent viscosity	1
Volume fraction	0.5	Energy	1

Euler-phase modelling are often accompanied by numerical instabilities and convergence problems. We chose a time step equal to 0.01 seconds when time steps was varies from 0.01 to 10 s. Although this step is less accurate, for example, a part of study used time step equal to 10-4 s, we decide that this compromise was necessary due to the lack of the high-performance computer and time. Real terms of these studies take time up to 3 months. The modeling time was 50 s, which is much longer than the average FCC residence time (2–3 s) in FCC unit [10] to stabilize the results, since more time was required to converge of the solution. The actual time of the modeling was about 6 hours for this study.

The main aim of this study, is to mix the different phases for occurring chemical reactions. The following key parameters characterize the mixing velocity: the value and distribution of the velocity, the volume fraction of the phase as well as the retention of the solid. The current section presents the results according to these key parameters after modelling.

The velocities of the solid and gas phases vary in a wide range according to Fig. 2. The velocity of the solid phase changes from 1 to 9 m/sin the nozzle and the accelerating section of the riser. When this phase reaches the feedstock injection zone, velocity rises up to 50 m/s due to a high feedstock velocity. Given that the catalyst flows by gravity through the pipe, the volume fraction does not exceed 0.44 in its upper part. In addition, the volume fraction is 0.55 before the feedstock input due to the low steam velocity, which raises the catalyst to the top. The volume fraction of the catalyst after the feedstock input zone is significantly reduced, reaching 0.2. This stems from a high feedstock velocity at the nozzles outlet of the which significantly accelerates the catalyst particles.

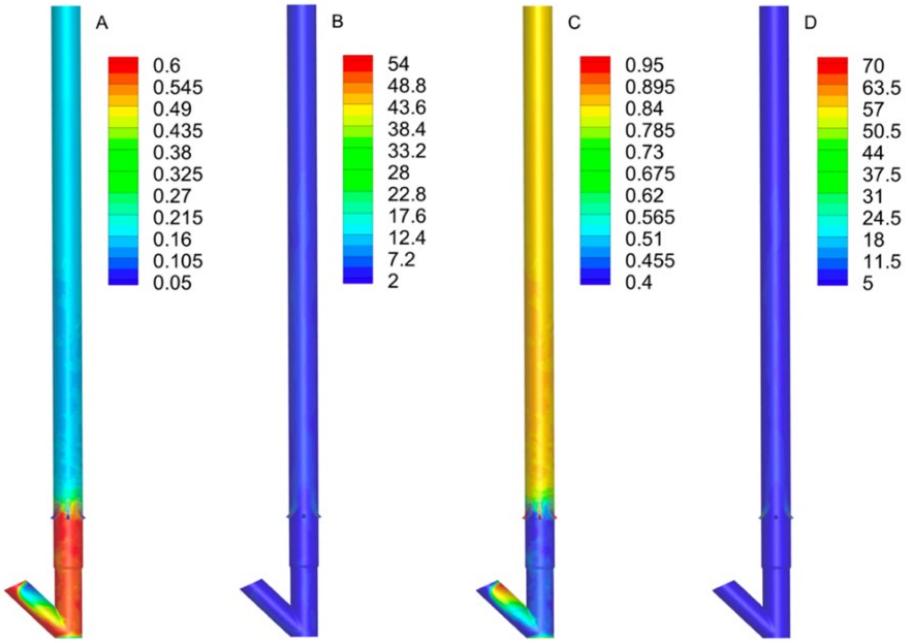

Figure 2. The main profiles of the solid and gaseous phases

A is the distribution of the solid phase volume fraction; B is the distribution of the solid phase velocities (m/s); C is the distribution of the gaseous phase volume fraction; D is the distribution of the gaseous phase velocities (m/s)

Fig. 3 shows that the temperature of the catalyst (A), passing through the riser, decreases from 975 K to 972 K and 969 K, when the height of the riser is 9 m and 36 m, due to heat exchange with the feedstock. Given that the feedstock was specified as a mixture (vacuum gas oil and water vapor) (Tables 3, 4), the temperature varies in the range from 350 to 479 K for water vapor, and from 733 to 780 K for vacuum gas oil from the level of the nozzles in the lower part of the riser.

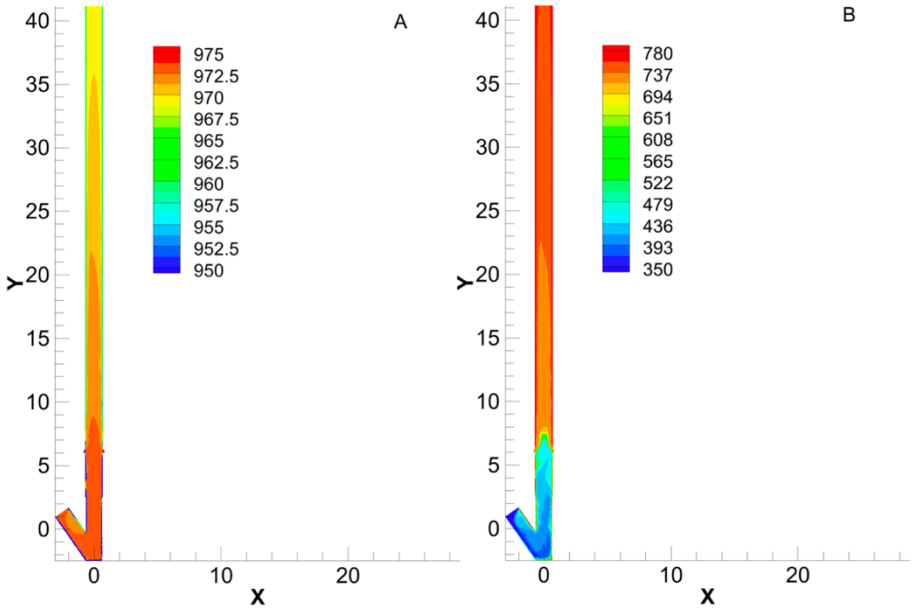

Figure 3. Temperature distribution profiles
A is the temperature distribution of the solid phase; B is the temperature distribution of the gaseous phase

3. Results and discussion

3.1. Comparison of the results obtained

Before comparing the present and Yang et al. results, we analyzed how their model differs from the model created in this study. Their riser geometry mainly differs in two features: i.e. the nozzles for slops was added at the top of the riser; and the group of nozzles was added further up the column to achieve control of the mixture temperature (MTC nozzles). The latter is necessary to maintain a constant pressure when the reactions with the formation of cracking products occurs.

The volume fraction of the regenerated catalyst is kept constant and the inlet velocities are the same for all components However, the Yang et al. model considers the huge number of cracking reactions occurring at the FCC riser. Moreover, HPC was used by Yand et.al, which ran only 30 seconds of flow modelling in 3 months. This helped to take a much smaller time step, which allowed them to obtain more accurate results.

One of the main tracked parameters for Yang et.al. was a catalyst velocity profile, when a solid is strongly accelerated almost equally on both sides of the riser wall. This led to decrease in the velocity values in the middle of the cross section, which disappears when the flow moves upward. Such increase in flow uniformity over the studied geometries stems from mainly two reasons: addition of a plurality of feed injection nozzles, which were evenly distributed over the column diameter; and adding MTC nozzles at the top of the riser.

These factors mainly compensate that the regenerated catalyst was introduced into the column from the left, which should have increased its velocity near the right riser wall. The average velocity profile is similar to Yang et.al, including its uniformity, when the flow increased.

The volume fraction profiles obtained by Yang *et.al.* indicate a significant solids retention under the feed nozzles. This is very similar to Figure 4 (A) and provides that this geometry accurately reflects accumulation of phases in the actual FCC process. Both profiles show that a catalyst volume fraction are a shade less 0.6 throughout the regenerated catalyst pipe and this value is low significantly after injection of the high-velocity flow of the feedstock.

The distribution of the solid phase temperature obtained by Yang et.al shows that the temperature of the solid phase when the feedstock inputs decreases from 973 K to 853 K. In the present study, a temperature is not decreased due to the absence of slops nozzles at the top of the riser. However, the trend of the temperature decreasing is similar to Yang et.al.

3.2 Hydrodynamic model of S-200, KT-1/1 catalytic cracking unit

Given that the developed model shows a high convergence with the results presented by Yang et.al., the next step of this study is the change of the operating and boundary conditions using the values of the S-200, KT-1/1. We used the mass flowrate as the boundary conditions for each inlet since the values of the velocities at the inlet were not known. The boundary conditions are presented in Table 8.

Table 8. The boundary conditions for the S-200, KT-1/1

Parameter	Value
Inlet Feed	
Feed for 4 nozzles mass flow rate, kg/s	63.30
Feed volume fraction	1
Feed temperature, K	682
Inlet Water-vapor	
Water-vapor mass flow rate, kg/s	0.83
Water-vapor volume fraction	1
Water-vapor temperature, K	582
Inlet Catalyst	
Catalyst mass flow rate, kg/s	533.47
Catalyst volume fraction	0.6
Catalyst temperature, K	922

Modelling of the riser using S-200, KT-1/1 operating variables showed that a solid phase distribution occurs with a significantly lower volume fraction (Fig. 4 (A)) in comparison with the results obtained under the operating conditions of the Yang et.al. This stems from the catalyst consumption, which are 533 and 1740 kg/s for present study of S-200 KT-1/1and Yang results respectively.

In the upper part of the riser when the feedstock inputs to the riser, the catalyst volume fraction reduces considerable, reaching 0.16, due to the high feed velocity, which reaches 95 m/s at the exit from injectors (Fig. 4 (D)) accelerating significantly the catalyst particles.

In addition, the catalyst volume fraction before the feedstock injection zone is 0.44 due to the low steam velocity, which raises the catalyst to the top. This can be explained by the fact that the steam velocity remains practically at the same level as Yang et.al results, when the catalyst flowrate is significantly lower. The catalyst does not have time to accumulate in large quantities. The catalyst velocity significant increases from 50 m/s to 70 m/s, when it achieves the level of the feedstock injection.

Fig. 5 shows that the catalyst temperature (A) decreases from 922 K to 917 K and to 908 K when the riser height increases from 20 m to 40 m respectively. This springs from heat exchange with the feedstock. In the riser bottom, the temperature varies in the range from 630 to 663 K for the steam, and from 634 to 718 K for the feedstock.

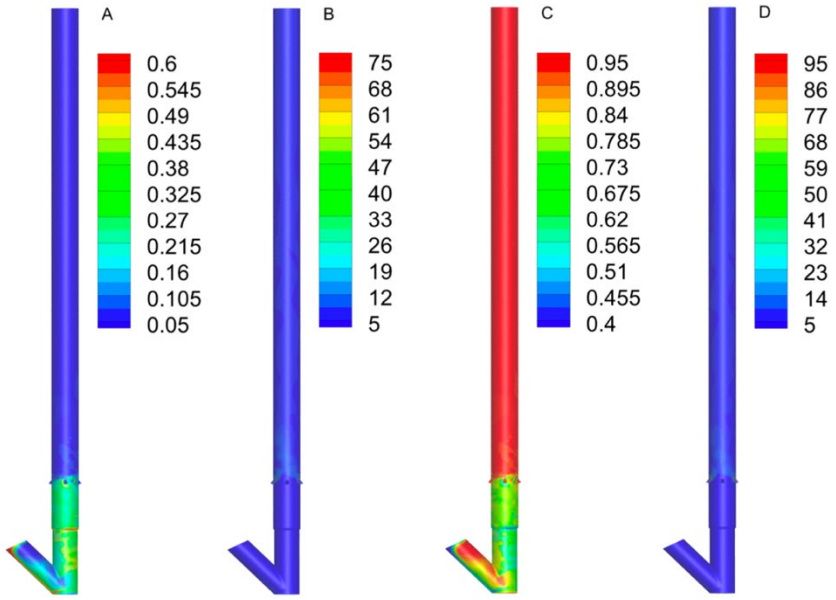

Figure 4. The main profiles of the solid and gas phase in riser of the S-200 KT-1/1 unit
A is the distribution of the solid phase volume fraction; B is the distribution of solid phase velocities (m/s); C is the distribution of the gaseous phase volume fraction; D is the distribution of gaseous phase velocities (m/s)

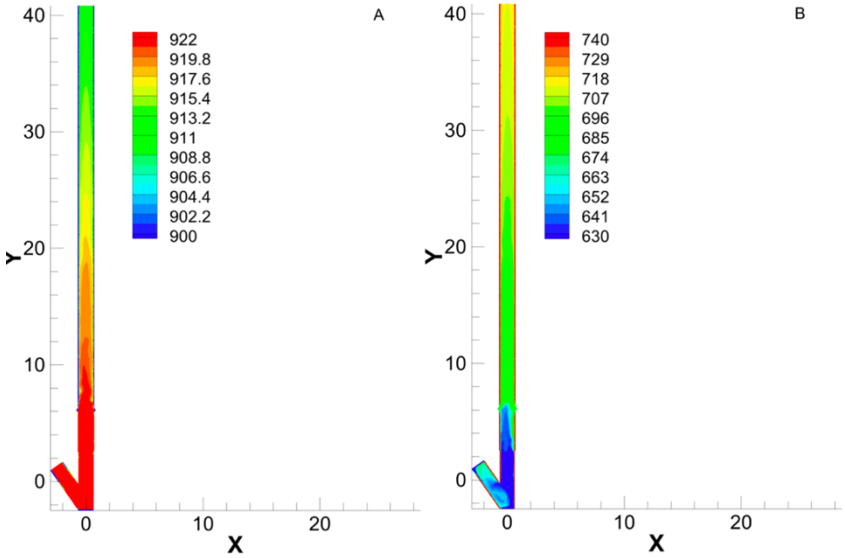

Figure 5. Profiles of temperature distribution in the riser of S-200, KT-1/1 unit
A is the solid phase temperature distribution; B is the gaseous phase temperature distribution

4. Conclusions

Through the 3D modeling of reactive two-phase flow using the Euler-Euler two-fluid model, a hydrodynamic model of the riser from S-200, KT-1/1 unit, was developed based on the geometry and productivity of a real industrial facility. This allows us to estimate how the distribution of temperature, velocity of catalyst and hydrocarbons by the riser height occurs considering hydrodynamic factors.

To predict the cracking temperature considering the heat of the reactions and the loss of kinetic energy, which has not been done previously, we are going to improve this model by more detailed description of the riser design, as well as the main chemical reactions of catalytic cracking. This will help us to study the distribution of the mass fractions of cracking products considering the hydrodynamics of the apparatus. The used methodology and the obtained

results should serve as guidelines for possible revision and optimization of the industrial process.

Acknowledgments

The reported study was funded by RFBR and RS, project number 21-53-10004.

Nomenclature

Greek and Roman letters

λ	Bulk viscosity
C	Carbon element
e	Coefficient of restitution
ρ	Density
k_{Θ_s}	Diffusion coefficient
ω	Drag force modify coefficient
d_s	Granular diameter
Θ	Granular temperature
g	Gravity
H	Hydrogen element
β	Interphase momentum transfer
ϕ	Kinetic energy transfer between two phases
P	Pressure
g_0	Radial distribution function
Re	Reynolds number
μ	Shear viscosity
C_p	Specific heat capacity
τ	Stress
t	Time
I	Unit tensor
$\vec{v}$	Vectoral velocity
ε	Volume fraction

Subscripts

g	Gas phase
n	Number of atoms
s	Solid phase
wt	Weight

References

[1] Amblard B, Singh R, Gbordzoe E, Raynal L. CFD modeling of the coke combustion in an industrial FCC regenerator. Chem. Eng. Sci. 2016; 170: 731-742.

[2] Weekman VW, Nace DM. Kinetics of Catalytic Cracking Selectivity in Fixed, Moving and Fluid-bed Reactors. AIChE. 1970; 16: 397–404.

[3] Jacob SM, Gross B, Weekman VM. A Lumping and Reaction Scheme for Catalytic Cracking A.I.Ch.E.J. 22: 701–703.

[4] Nazarova G, Ivashkina E, Ivanchina, E, Oreshina A, Vymyatnin E. A predictive model of catalytic cracking: Feedstock-induced changes in gasoline and gas composition. Fuel Process Technol. 2021; 217(5): 106720.

[5] Nazarova GY, Ivashkina EN, Ivanchina ED, Vosmerikov AV, Vosmerikova LN, Antonov AV. A model of catalytic cracking: Product distribution and catalyst deactivation depending on saturates, aromatics and resins content in feed. Catalysts. 2021; 11(6): 701.

[6] Nazarova G, Ivashkina E, Shafran T, Oreshina A, Seitenova G. Prediction of residue coke content and operating modes of regenerator in the catalytic cracking technology. Pet. Sci. Technol. 2020; 38(24): 1017–1025.

[7] Nazarova G, Ivashkina E, Ivanchina E, Oreshina A, Vymyatnin, E., Burumbaeva, G. Integrated mathematical modeling of catalytic cracking and zeolite-containing catalyst oxidative regeneration. Pet. Sci. Technol. 2020; 38(12): 754–762.

[8] Nazarova GY, Chuzlov VA, Ivanchina ED, Ivashkina EN, Kopycheva UN, Dolganova IO. Intellectual Training-System of the Process of Catalytic Cracking of Heavy Oils. Pet. Coal. 2020; 23: 1–21.

[9] Gan J, Zhao H, Abdallah S. Berrouk, Yang C, Shan H. Numerical Simulation of Hydrodynamics and Cracking Reactions in the Feed Mixing Zone of a Multiregime Gas–Solid Riser Reactor. Ind. Eng. Chem. 2011; 50(20): 11511-11520.
[10] Yang Q. CFD investigation of hydrodynamics, heat transfer and cracking reactions in a large-scale fluidized catalytic cracking riser. Appl. Math. Model. 2016; 40(21–22): 9378–9397.
[11] Gabriella C. Lopes, Leonardo M. Rosa, Milton Mori, Jose R. Nunhez, Wildir P. Martignioni CFD Study of Industrial FCC Riser: The Effect of Outlet Configurations on Hydrodynamics and Reactions. Chem. Engl. Science. 2016; 153: 58–74.
[12] Sheng Chen, Yiping Fan, Zihan Yan, Wei Wang, Xinhua Liu, Chunxi Lu. CFD optimization of feedstock injection angle in a FCC riser. Chem. Engl. 2012; 2012: 1–16.
[13] Huang W, Yan A, Zhu J Hydrodynamics and Flow Development in a 15.1 m Circulating Fluidized Bed Riser. Chem. Eng. Technol. 2007; 30(4): 460–466.
[14] Idris MN, Burn A. CFD Modelling Gas-Solid Flows in CFB/FCC Riser Reactors: Simulation Using Kinetic Theory of Granular Flow (KTGF) in a Fully Developed Flow Situation. AIChE. 2008.
[15] Barbosa A, Lopes G, Rosa L, Mori M, Martignoni W. Three Dimensional Simulation of Catalytic Cracking Reactions in an Industrial Scale Riser Using a 11-lump Kinetic. Chem. Eng. Trans. 2013; 32: 637-642.
[16] Gidaspow D. Multiphase flow and fluidization – Continuum and Kinetic. Academic Press Limited: Gardners Books, 1994; p. 467.
[17] Idris MN, Burn A. CFD Modelling Gas-Solid Flows in CFB/FCC Riser Reactors: Simulation Using Kinetic Theory of Granular Flow (KTGF) in a Fully Developed Flow Situation. American institute of chemical engineers. 2008; 16-21: 1-19.

To whom correspondence should be addressed: Dr. Vyacheslav Chuzlov, National Research Tomsk Polytechnic University, Engineering school of natural resources, Division for Chemical Engineering, Lenin Avenue, 30, Tomsk, 634050, Russia; e-mail: chuva@tpu.ru